The relationship of the magnetic properties of M (M = Mn, Fe, Co)-doped ZnO single crystals and their electronic structures

2009 J. Phys.: Condens. Matter 21 026009

(http://iopscience.iop.org/0953-8984/21/2/026009)

IOP PUBLISHING JOURNAL OF PHYSICS: CONDENSED MATTER

J. Phys.: Condens. Matter **21** (2009) 026009 (5pp) doi:10.1088/0953-8984/21/2/026009

The relationship of the magnetic properties of M (M = Mn, Fe, Co)-doped ZnO single crystals and their electronic structures

T Tamura and H Ozaki

Electrical Engineering and Bioscience, Waseda University, 3-4-1 Ohkubo, Shinjuku-ku, Tokyo 169-8555, Japan

E-mail: tkstmr@aoni.waseda.jp

Received 30 September 2008, in final form 31 October 2008
Published 9 December 2008
Online at stacks.iop.org/JPhysCM/21/026009

Abstract

The electronic density of states and magnetic properties were investigated by tunneling spectroscopy and SQUID, respectively, for a series of 3d transition-metal (Mn, Fe, Co)-doped ZnO. By tunneling spectroscopy an additional density of states was observed in Mn- and Co-doped ZnO adjacent to the top of the valence band of the host ZnO. Instead, in the Fe-doped sample, a band of density of states was observed across the Fermi level in the mid-gap. The magnetization curve (M versus H) obtained by SQUID showed a ferromagnetic hysteresis at room temperature for the Fe-doped sample, whereas for the Mn- and Co-doped samples, the M versus H curve showed only a linear characteristic without hysteresis. From the comparison of the density of states and the magnetization characteristics, it is strongly suggested that the ferromagnetism in Fe-doped ZnO at room temperature originates from the half-filled Fe 3d band in the mid-gap of the host ZnO.

1. Introduction

Diluted magnetic semiconductors (DMS), in which a portion of the atoms of the nonmagnetic semiconductor host is substituted by magnetic transition-metal ions, have attracted much interest in spintronics which exploits both the spin and the charge of carriers. In the last decade most of the investigations of DMS have focused on (Ga, Mn)As [1, 2] but the Curie temperature T_c was below room temperature, unsuitable for practical applications. Dietl *et al* predicted that p-type Mn-doped ZnO had a T_c above room temperature [3]. Since then ZnO has interested us in DMS which shows room temperature ferromagnetism and many workers have investigated the 3d-transition-metal-doped ZnO. There is, however, a lot of controversy about their results on the properties of magnetism and the origin of ferromagnetism [4–8]. With regard to the origin of ferromagnetism, two mechanisms have been proposed; one is the carrier-mediated mechanism [9] which is supported in (Ga, Mn)As, and the other is the bound magnetic polaron mechanism [10]. However, ferromagnetism has been observed in both the degenerate semiconductor range and the insulator range, and thus the ferromagnetism cannot be explained by any one of these mechanisms. In regard to the electronic structure of doped magnetic ions in ZnO, some theoretical investigations have been reported [11–14], but systematic experimental studies are very few up to now. Therefore, it is very important to know the fundamental properties of magnetic impurities in ZnO in order to elucidate the origin of the ferromagnetism.

In this study we have observed the electronic density of states (DOS) of a series of 3d transition-metal (Mn, Fe, Co)-doped ZnO by tunneling spectroscopy, which is one of the useful methods for analyzing the DOS directly with high resolution, and they were compared with recent theoretical results. Also, we have measured the magnetic properties of the samples at room temperature and investigated the relationship of the electronic structures and the magnetic properties.

2. Experiments

Single crystals of non-doped and M-doped ZnO (M = Mn, Fe, Co) were prepared by the chemical vapor transport (CVT)

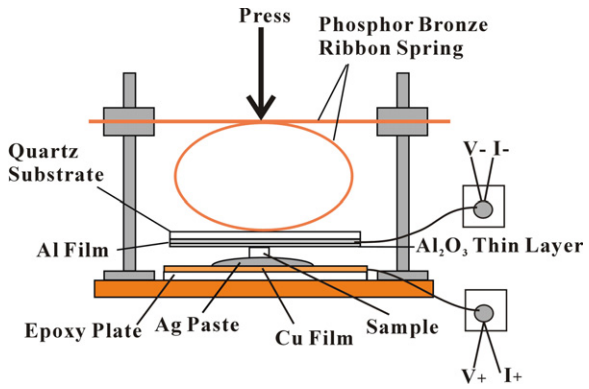

Figure 1. Schematic planar-contact tunnel junction employed in this study.

(This figure is in colour only in the electronic version)

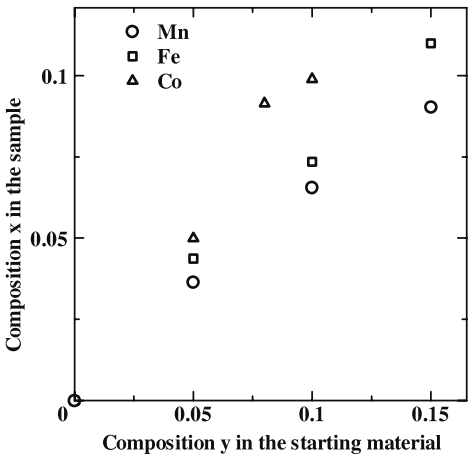

Figure 2. The relationship of the M (=Mn, Fe, Co) composition x in the sample $M_xZn_{1-x}O$ and the composition y in the starting material.

Table 1. Growth conditions of CVT.

Sample	Transport agents	T_1 (K)	T_2 (K)	Growth time (h)
ZnO	$ZnCl_2$	1373	1073	120
$Zn_{0.910}Mn_{0.090}O$	$ZnCl_2 + C$	1253	1153	120
$Zn_{0.890}Fe_{0.110}O$	NH_4Cl	1323	1073	120
$Zn_{0.909}Co_{0.091}O$	$ZnCl_2$	1373	1073	120

method [15–17]. The 4N-purity ZnO powder was mixed with 3N-purity Mn_3O_4 powder for Mn doping, 3N-purity FeO powder for Fe doping and 3N-purity Co_3O_4 powder for Co doping. Then pellets of 13 mm diameter were prepared by pressing the mixed powders at 500 MPa for 10 min and sintered at 1273 K for 10 h in the atmosphere. Exceptionally, Fe-doped ZnO pellets were sealed in quartz ampoules under 10^{-3} Pa and sintered at 1273 K for 10 h. The resultant pellets were a single phase of wurtzite. After the sintering, pellets were crushed and sealed in quartz ampoules of 200 mm (long) × 10 mm (diameter) under 10^{-3} Pa together with transport agents. The sealed ampoules were set across the border of the source zone and the growth zone of an electric furnace for single-crystal growth.

Table 1 shows the transport agents, temperatures of the source zone (T_1) and the growth zone (T_2), and the time of growth for samples used in this study. The structural characterizations of the samples were made by x-ray diffraction and the Laue method, and the M composition x in $M_xZn_{1-x}O$ was determined by energy-dispersive x-ray spectroscopy (EDX).

The as-grown crystals usually contain defects of oxygen vacancies and/or interstitial Zn, which provide the sample with conduction electrons. Hereafter we refer the defects to these kinds. In order to remove these defects, samples were annealed before the measurements.

Tunneling measurements were carried out at room temperature using an Al/Al_2O_3/sample planar-contact structure. First, Al was evaporated onto a quartz substrate. Then it was heated in the evaporation chamber at about 423 K for 1 h in O_2 atmosphere of 1 atm to oxidize the Al surface. The Al_2O_3 surface thus prepared was pressed against the sample surface using a phosphor–bronze ribbon spring to form a stable-contact tunnel junction, as shown in figure 1. The pressure applied to the tunnel junction was adjusted so as to make the electrical resistance of the tunnel junction much higher than that of the sample bulk resistance in series with the tunnel resistance, in order to minimize the error in the tunnel bias voltage. Within the range of pressure applied in this study, a pressure-dependent change in the tunneling spectra was not observed. The tunnel bias voltage is defined here as the potential of the sample against that of Al metal. The theory of tunneling spectroscopy was briefly described in the previous study [18].

Magnetic properties were measured by using the superconducting quantum interference devices (SQUID) with magnetic field in the range ±3000 Oe applied perpendicular to the (100) plane of the sample.

3. Results and discussion

The shape of the grown crystal samples was a hexagonal pillar, and by the Laue method, samples were confirmed to be wurtzite single crystal. Figure 2 shows the M (=Mn, Fe, Co) composition x in the sample $M_xZn_{1-x}O$ versus the composition y in the starting material. x was obtained by taking the average of measured values at several different positions on the sample surface. The dispersion of x values for each measurement was within ±1%. x increased almost linearly up to 0.09 for Mn, 0.11 for Fe and 0.10 for Co on increasing y. In order to examine whether there is a secondary phase in the sample, we powdered the sample and measured the XRD patterns. As shown in figure 3(a), the XRD patterns were totally assigned to ZnO wurtzite and the secondary phase was not detected. The cell volume from XRD increased, as shown in figure 3(b), almost linearly with the M composition for Mn and Fe according to the difference of those ionic radii and that of the Zn ion. For the Co-doped sample, the cell volume slightly decreased for small x, but it increased for larger x in spite of the smaller ionic radius of Co than that of Zn. It might happen due to the interstitial occupation of Co ions for larger x.

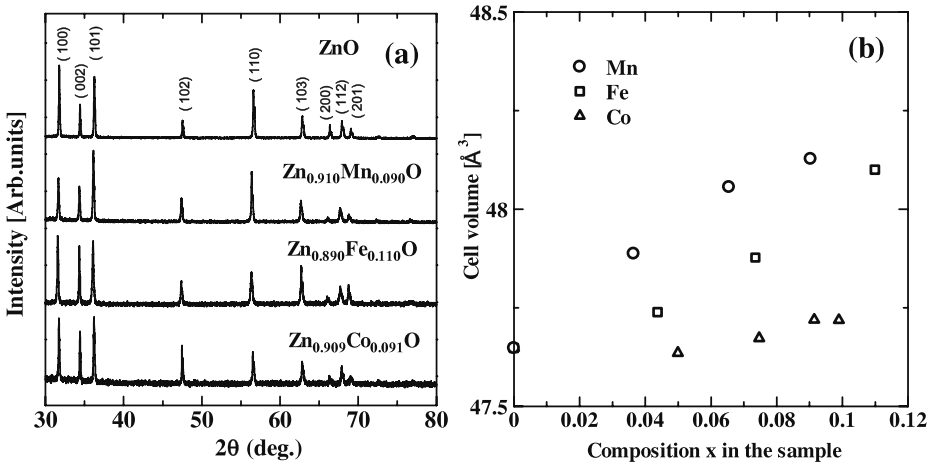

Figure 3. (a) XRD patterns of non-doped and M-doped ZnO samples after powdering and (b) the cell volume as a function of the composition x in the sample.

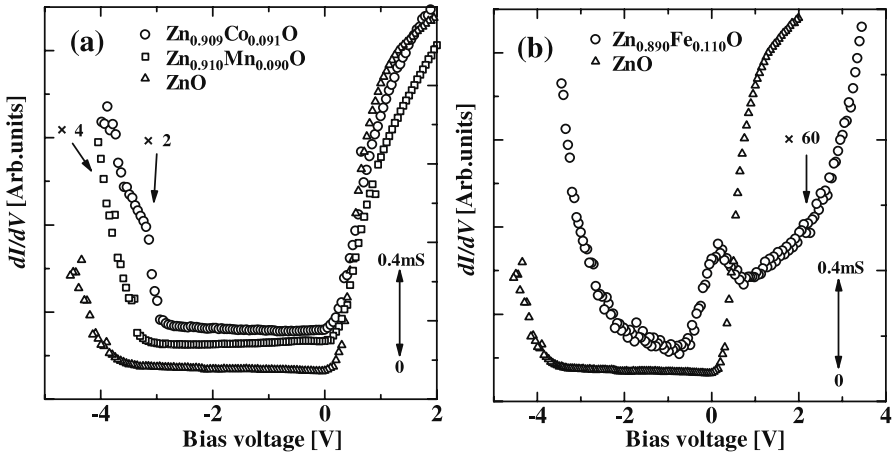

Figure 4. (a) Tunneling spectra for $Zn_{0.910}Mn_{0.090}O$, $Zn_{0.909}Co_{0.091}O$ and non-doped ZnO, and (b) for $Zn_{0.890}Fe_{0.110}O$ and non-doped ZnO.

3.1. Tunneling spectra for non-doped and doped ZnO

Figure 4(a) shows the tunneling dI/dV versus V characteristics for non-doped, Mn- and Co-doped samples. As shown in figure 4(a), the tunneling spectrum for non-doped ZnO shows sudden rises at around 0 and −3.4 V. In short, the bandgap (the separation of the two rises) is 3.4 eV and the Fermi level (ε_F: bias voltage 0) is just at the conduction band bottom edge, which illustrates a strong n-type. The temperature dependence of resistivity (ρ) for 20 K $< T <$ 300 K and the Hall coefficient at room temperature were measured for the non-doped sample. The carrier concentration (n-type) at room temperature was 4×10^{17} cm^{-3} and the activation energy of resistivity derived from the lower temperature region of the ρ–T curve was 9 meV. Such a strong n-type seems to be introduced by the interstitial Zn and/or substituted Cl for O from the transport agent $ZnCl_2$ as well as by O vacancies. Similar tunneling measurements were performed using Al_2O_3 tunnel barriers with various thicknesses and the above value of the energy gap (3.4 eV) was reproduced, which means that the voltage drop across the series resistance due to the sample bulk was negligible in the experiments.

For Mn- and Co-doped samples, the rises in the DOS were observed in the tunneling spectra around 3.2 eV and 2.8 eV below the bottom of the conduction band near the Fermi level (ε_F), respectively. These behaviors are in qualitative agreement with the theoretical results that the 3d-t_{2g} band lies just above the top of the valence band [11, 13]. The theoretical results indicate the existence of another 3d band in the conduction band: however, the present experiments could not identify this DOS.

For the Fe-doped sample, as shown in figure 4(b), the tunneling spectra showed a very different behavior from those in the non-doped and Mn- and Co-doped samples shown in figure 4(a). A band of DOS with about 1.2 eV width was observed across ε_F (bias 0). The transition-metal 3d band with similar width (∼1.5 eV) was observed by photoemission in V-doped ZnO [19]. The onset of rises in the DOS on the negative and positive sides of the bias were around −2.1 eV and 2.3 eV, respectively. The theoretical results showed a narrower DOS in the mid-gap of Fe-doped ZnO: some of them showed it below the Fermi level [11, 12] and some others showed it on the Fermi level [13]. Theoretically, this narrow DOS was assigned to the minority-spin 3d-e_g band.

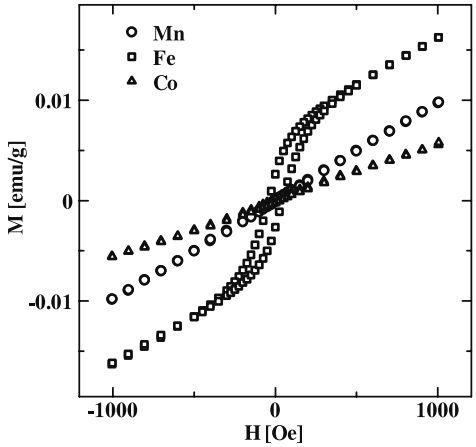

Figure 5. The M–H curves at room temperature for $Zn_{0.910}Mn_{0.090}O$, $Zn_{0.890}Fe_{0.110}O$ and $Zn_{0.909}Co_{0.091}O$, for which tunneling measurements were carried out.

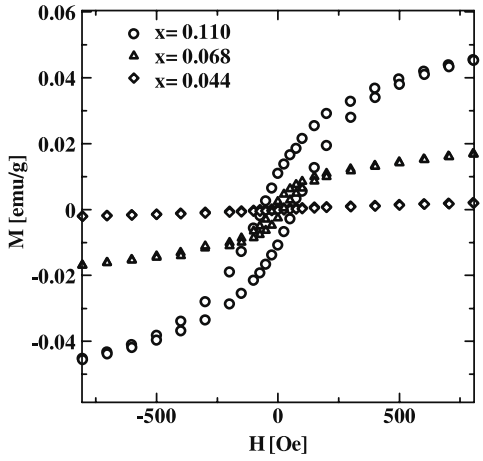

Figure 7. The M–H curves for various x in $Zn_{1-x}Fe_xO$ at room temperature after annealing at 973 K for 10 h.

3.2. Magnetic properties of doped ZnO

Figure 5 shows the magnetization (M) versus the magnetic field (H) curves at room temperature for Mn-, Fe- and Co-doped samples which were annealed under the same conditions as those for the tunneling measurements. The M–H curve for the Fe-doped sample showed a hysteresis loop but not for the Mn- and Co-doped samples. We consider that these differences were caused by the difference in the position of the ε_F in ZnO. For the Fe-doped sample, since the ε_F is on the Fe 3d level in the mid-gap, as shown in figure 4(b), electrons may hop between the Fe 3d levels. On the other hand, for Mn- and Co-doped samples, since the ε_F is just below the bottom of the ZnO conduction band, whereas the 3d levels lie just above the ZnO valence band, as shown in figure 4(a), the carrier transport does not occur on the 3d levels. In short, these differences strongly influence the magnetic properties of each M-doped ZnO. For the magnetic property measurements, samples were fully annealed (10 h, 20 h) in order to remove the whole of the defects in the bulk.

Figures 6(a) and (b) show the M–H curves and the saturation magnetization for several annealing times, respectively. The saturation magnetization was obtained by extrapolating the linear portion of the M–H curve at high magnetic field up to 3000 Oe (not shown in figure 6(a)) to $H = 0$. The hysteresis loop increased with increasing the annealing time and the saturation magnetization increased linearly with annealing time. On the other hand, the slope of the M–H curve at higher magnetic field was almost unchanged with annealing time. It indicates that this latter effect is not associated with the defects (oxygen vacancies and/or interstitial Zn) which was reduced by the annealing. On decreasing the defects by the annealing the M became larger. But there seemed still some defects left in the sample after the annealing at 973 K for 20 h because the saturation magnetization still did not converge. The as-grown samples contain the defects, which supply the 3d states with electrons. It is thus considered that not all the Fe ions contribute to the ferromagnetism but the minority-spin 3d-e_g state of some Fe ions are still filled with electrons from the defects and are well below the Fermi level even after the annealing carried out in this study.

Figure 7 shows the Fe composition dependence of the M–H curve. The saturation magnetization and the slope of the

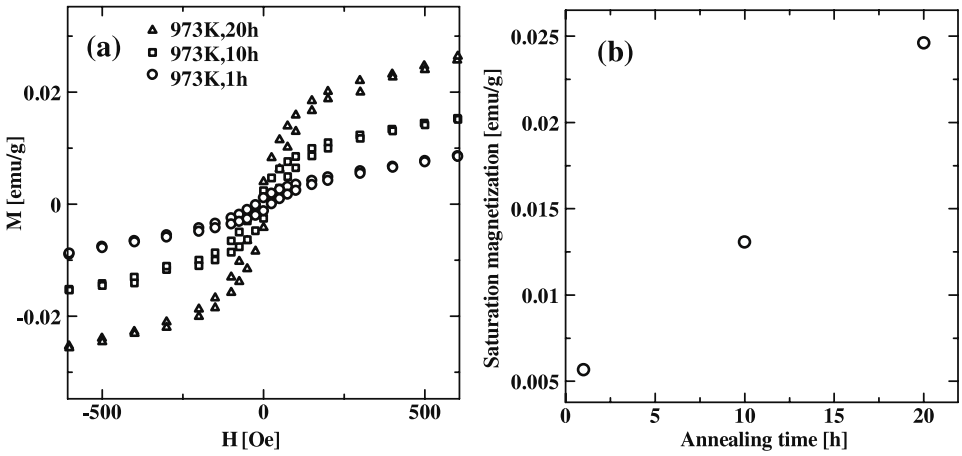

Figure 6. The M–H curves (a) and the saturation magnetization (b) of $Zn_{0.932}Fe_{0.068}O$ at room temperature for several annealing times.

M–H curve at higher magnetic field increased with increasing Fe composition. By these results we also consider that the slopes are influenced by the Fe ions and not by the defects. The M increased linearly with increasing H up to 3000 Oe without any sign of saturation.

From all the above experimental results, it is strongly suggested that the ferromagnetism of Fe-doped ZnO at room temperature originates from the electrons in the minority-spin 3d-e_g band at the Fermi level, which means that the electrons are somewhat delocalized. In Mn- and Co-doped ZnO, this band is empty and full, respectively. Therefore, there is no partially filled 3d band, and thus the ferromagnetism is not caused. A preliminary M–T measurement suggests that the filled majority-spin 3d bands, together with the filled minority-spin 3d-e_g band if any, might lead to a linear characteristic in the M versus H curve.

Investigations on co-doping of an acceptor with Mn and Co will be important for a precise understanding of the mechanism of ferromagnetism in this system.

4. Summary

The electronic density of states and the magnetic properties were investigated by tunneling spectroscopy and SQUID, respectively, for a series of 3d transition-metal (Mn, Fe, Co)-doped ZnO.

An additional density of states was observed in Mn- and Co-doped ZnO adjacent to the top of the valence band of the host ZnO, and the samples were strongly n-type. Instead, in the Fe-doped sample, a band of density of states with 1.2 eV width was observed across the Fermi level in the mid-gap.

The magnetization curve (M versus H) obtained by SQUID showed ferromagnetic hysteresis at room temperature for the Fe-doped sample superimposed on a linear characteristic, whereas for Mn- and Co-doped samples, the M versus H curve showed only the linear characteristic without hysteresis.

Both the size of the hysteresis (saturation magnetization and coercive force) and the slope of the linear characteristics increased with the Fe composition.

From the comparison of the density of states and the magnetization characteristics, it is strongly suggested that the ferromagnetism in Fe-doped ZnO at room temperature originates from the partially filled Fe 3d band in the mid-gap of the host ZnO.

References

[1] Ohno H, Shen A, Matsukura F, Oiwa A, Endo A, Katsumoto S and Iye Y 1996 *Appl. Phys. Lett.* **69** 363

[2] Jungwirth T, Wang K Y, Mašek J, Edmonds K W, König J, Sinova J, Polini M, Goncharuk N A, MacDonald A H, Sawicki M, Rushforth A W, Campion R P, Zhao L X, Foxon C T and Gallagher B L 2005 *Phys. Rev.* B **72** 165204

[3] Dietl T, Ohno H, Matsukura M, Cibert J and Ferrand D 2000 *Science* **287** 1019

[4] Sharma P, Gupta A, Rao K V, Owens F J, Sharma R, Ahuja R, Osorio-Guillen J M and Gehring G A 2003 *Nat. Mater.* **2** 673

[5] Ueda K, Tabata H and Kawai T 2001 *Appl. Phys. Lett.* **79** 988

[6] Jung S W, An S J, Yi G C, Jung C U, Lee S and Cho S 2002 *Appl. Phys. Lett.* **80** 4561

[7] Yoon Y W, Cho S B, We S C, Yoon B J, Suh S, Song S H and Shin Y J 2003 *J. Appl. Phys.* **93** 7879

[8] Fukumura T, Jin Z, Kawasaki M, Shono T, Hasegawa T, Koshihara S and Koinuma H 2001 *Appl. Phys. Lett.* **78** 958

[9] Priour D J Jr, Hwang E H and Sarma S D 2004 *Phys. Rev. Lett.* **92** 117201

[10] Coey J M D, Venkatesan M and Fitzgerald C B 2005 *Nat. Mater.* **4** 173

[11] Toyoda M, Akai H, Sato K and Katayama-Yoshida H 2006 *Physica* B **376/377** 647

[12] Gopal P and Spaldin N A 2006 *Phys. Rev.* B **74** 094418

[13] Debernardi A and Fanciulli M 2007 *Appl. Phys. Lett.* **90** 212510

[14] Janisch R, Gopal P and Spaldin N A 2005 *J. Phys.: Condens. Matter* **17** R657

[15] Ntep J M, Hassani S S, Lusson A, Carli A T, Ballutard D, Didier G and Triboulet R 1999 *J. Cryst. Growth* **207** 30

[16] Matsumoto K, Konemura K and Shimaoka G 1985 *J. Cryst. Growth* **71** 99

[17] Matsumoto K and Shimaoka G 1988 *J. Cryst. Growth* **86** 410

[18] Tamura T, Kim C, Oikawa Y and Ozaki H 2007 *MRS 2007 Fall Proc. (Boston, Nov. 2007)* vol 1035E, pp 1035-L05–26

[19] Ishida Y, Hwang J I, Kobayashi M, Fujimori A, Saeki H, Tabata H and Kawai T 2004 *Physica* B **351** 304